TABLE OF CONTENTS (TOC)

Direct LED writing of submicron resist patterns: towards the fabrication of individually-addressable InGaN submicron-stripe LED arrays

Z. Gong [a,b,*], B. Guilhabert[a], Z.T. Chen[b], and M.D. Dawson[a]

[a]Institute of Photonics, University of Strathclyde, Wolfson Centre, 106 Rottenrow, Glasgow G4 0NW, UK.

[b]Guangdong General Research Institute for Industrial Technology,No.363, Changxin Road, Tianhe District, Guangzhou 510650, China

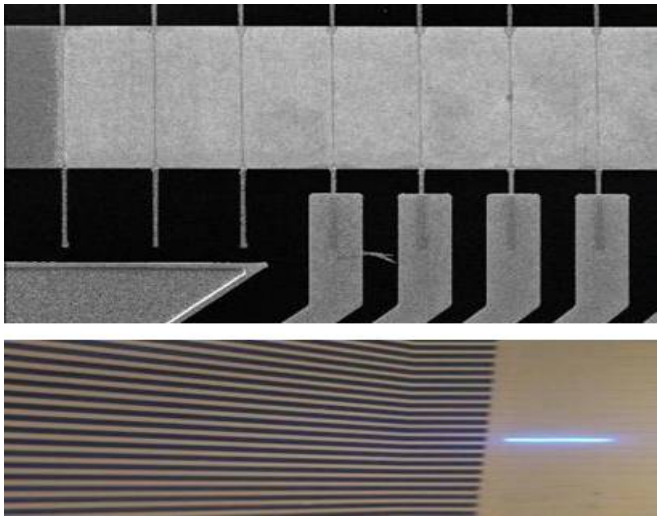

Individually addressable Submicron-stripe LEDs manufactured by a novel technique based on direct LED writing was reported

Insitute of Photonics, University of Strathclyde, G4 0NW, UK.
Zheng Gong, zheng.gong@mled-ltd.com

TSINGHUA UNIVERSITY PRESS Springer

Nano Research
DOI (automatically inserted by the publisher)
Review Article/Research Article **Please choose one**
ISSN 1998-0124
CN 11-5974/O4

Direct LED writing of submicron resist patterns: towards the fabrication of individually-addressable InGaN submicron stripe-shaped LED arrays

Z. Gong[a,b,c](✉), B. Guilhabert[a], Z.T. Chen[b] , and M.D. Dawson[a]
[a] *Institute of Photonics, University of Strathclyde, Wolfson Centre,106 Rottenrow, Glasgow G4 0NW, UK.*
[b] *Guangdong General Research Institute for Industrial Technology, No.363,Changxin Road, Tianhe District, Guangzhou 510650, China*
[c] *Current address: mLED Ltd., 50 Richmond Street,Glasgow G1 1XP, UK.*

Received: day month year
Revised: day month year
Accepted: day month year (automatically inserted by the publisher)

KEYWORDS

Direct writing;
light-emitting diodes;
electroluminescence;
efficiency droop;
mask-free lithography

ABSTRACT

Submicron stripe-shaped InGaN LED arrays with individually addressable capabilities are demonstrated. The critical submicron-stripe metallic electrodes, which define the emission pattern, are formed by direct LED writing in a mask-free manner. The individually addressable submicron-stripe LED shows excellent performances in terms of the electric characteristics (with typical turn-on voltage of 3V, operation stability and power output up to 28μW at 3mA). Unlike conventional broad-sized LEDs, the efficiency droop of the submicron-stripe LED is significantly suppressed—in fact, there is no efficiency droop under current densities up to 100A/cm^2. Furthermore, the submicron-stripe LED shows less temperature-dependent shift of the emission wavelength. The lateral emission width is increased with increasing the injection current, resulting in a wider lateral emission size than the metallic submicron-stripe electrode. The underlying physics for these phenomena are analysed. Such submicron-stripe LED arrays open up the promising applications in nanophotonics and bio-sensing.

Introduction

The invention of light-emitting diodes (LEDs) has led to significant changes in our daily life. Solid lighting industry is undergoing rapid development since the advent of high-brightness GaN LEDs [1]. These LEDs generally have large die sizes (300μm or above), in order to deliver high enough irradiance for illumination purposes. On the other hand, there are some potential applications for which very tiny light sources with sizes approaching one micron or below are needed, such as near-field scanning optical microscopy [2], nano-lithography [3], and single molecules excitation [4]. These applications have motivated intensive investigations of nanoscale emitters over the past decade. So far, various nanoLEDs based on different semiconductor materials such as organic light emitting polymers [5–10], ZnO [11–14], InP [15], GaMnAs/GaAs [16], and InGaN/GaN [3,17,18] have been demonstrated, thanks to continuous advances in epitaxial growth and lithographic techniques. Inorganic semiconductor nanoLEDs are particularly interesting because they are expected to have better device performances than organic counterparts in terms of the device reliability and brightness.

Recent progress toward nanoLEDs has been mainly achieved by shrinking LED sizes, forming nanoscale p-n junctions, and positioning electrodes [2–18]. So far, various techniques have been utilized to fabricate nanoLEDs, among which electron-beam lithography is most widely used [6,7]. E-beam lithography allows features down to a few nm to be accurately produced. However, the high cost and low production efficiency are still the main shortcomings limiting their practical application for wafer-scale production. Alternatively, other more cost-effective techniques have been also developed. For instance, Makarovsky et al. used a direct non-destructive laser writing technique to produce a nanoLED by spatially controlled diffusion of mobile interstitial manganese (Mni) donor ions out of the ferromagnetic semiconductor $Ga_{1-x}Mn_xAs$ towards the underlying layers of a quantum well (QW) heterostructure [16]. This method, however, may be only suitable for specific semiconductor material systems. Price et al. demonstrated the use of phase-shifting lithography to manufacture high-density, large-area organic nanoLEDs [5]. However, each nanoLED was unable to be individually addressable, due to the fact that there is no separate electrode for each pixel. Veinot et al. disclosed a smart method to produce organic nanoLEDs with size down to 40nm by using nanosphere lithography [6]. However, the spatial distribution (i.e., hexagonal arrangement) of the nanoLEDs is unable to be routinely changed, due to the self-assembly nature of colloidal nanoparticles. Motayed et al. demonstrated the use of dielectrophoresis to assembly n-GaN nanowires onto p-GaN to achieve electrically excited 365 nm emission [14]. While the device fabricated by this method indeed constitutes a real nano-emitter, the positions of these nanowires are unable to be controlled accurately, making their routine use in integrated devices difficult. To date, the fabrication of truly individually-addressable nanoLED array with precise size and position control still remains challenging. Furthermore, these demonstrated devices to date show compromised device operation performance, with either high turn-on voltage (typically in the range of 4-15v. see refs [3, 4, 6] for example.), poor I-V characteristics (the typical current is from 100 nA to 3uA at 8~20V. See refs [3-9].), or very weak emission (in most cases, only EL is recorded for these devices while no optical power is documented), making them difficult for realistic applications.

In this paper, we report a novel method based on direct LED writing to manufacture high performance InGaN/GaN submicron-stripe LED arrays. The array nature of the submicron-stripe devices renders them more functionality such as pattern-programmable capability, which would be impossible for single nanoLED. ~10μm feature size has been achieved by direct LED writing previously [19–21]. Here we extend this technique to realize submicron scale resolution lithography. The critical sub-micron scale electrodes are formed by evaporating Ni/Au onto LED-written nano-scale resist patterns followed by metal lift off. The submicron-stripe LED arrays manufactured by this technique, compared with those aforementioned, have many merits including: (i) precise control of individual submicron-stripe LED size and position, (ii) robust device operation (no obvious brightness degradation within 2-day CW operation at a current

density of 1.1KA/cm²), improved I-V characteristics (the injection current can be up to 3mA, at least one order higher than earlier devices. The turn-on voltage is only 3V, which is comparable to conventional GaN LEDs), and substantially improved brightness (the measured power is up to 28uW per pixel), (iii) individually addressable capability, and (iv) simple device fabrication procedure without complicated pattern multi-registration. Such high performance submicron-stripe LED arrays open up a wide range of practical applications such as sensors, and single molecular excitation.

Results and discussion

The LED writing system is adapted from the one that we have reported previously [21]. The main components of the LED writing system include a CMOS-controlled UV LED array, an optical imaging system, and a sample X-Y moving stage(**Supporting Information, Figure S1**). The original LED writing system only has a lithography resolution of ~8μm. In order to realize sub-micron scale lithography, a new 8x8 370nm-emiting CMOS-driven InGaN LED array with different pixel sizes ranging from 14μm to 84μm (**Supporting Information, Figure S2**) and an optical 10x de-magnification imaging system (a 4x collection objective and a 40x projection objective) are introduced. Thus, the projected spot size (on the sample surface) is significantly reduced (the spot size is approximately from 1.4μm to 8.4μm, corresponding to a LED pixel size of 14μm to 84μm). By projecting the UV emission onto the surface of the sample coated with photoresist, a pattern can be directly written into the photoresist layer in a mask-less manner. The practical writing process is automatically implemented through a computer interface. A more detailed description of the LED writing system has been reported in ref. [21]. Based on this system, sub-micron features are readily achieved. The AFM image shown in **Figure 1a**, for example, illustrates a trench formed into the S1805 resist layer by switching on a 14μm pixel in the UV LED array, and by moving the sample at a speed of 140μm/s. A Feature size down to 800nm has been achieved for this specific experiment. In the case of negative resist ma-N405, a feature size of 1.2μm is obtained, as shown in Figure 1b. Actual feature size after exposure is dependent on the pixel size and the velocity of the sample moving stage. A distinct merit of our LED writing system from others is that parallel writing using multi-pixels from the LED array can be executed, due to the programmable capability of the CMOS driven LED array.

Considering that the LED writing system has a submicron writing resolution, we now use it for the fabrication of nano-scale LEDs based on 460nm GaN LED wafers. For purpose of illustration, a 1-D submicron-stripe LED array is fabricated based on the LED writing system, in conjunction with conventional optical lithography. The device processing flow is schematically shown in **Figure 2**. The device fabrication starts by creating a SiO_2 window (Figure 2b) in a LED wafer (Figure 2a) coated with a SiO_2 layer. Then the sample is coated with a photoresist layer, followed by LED writing, to define the critical nano-stripe resist pattern (Figure 2c). A Ni/Au metal layer is then evaporated onto this patterned resist layer, followed by metal lift off, to form Ni/Au submicron-stripes across the SiO_2 window (Figure 2d). The following step is to expose n-GaN by ICP dry etching (Figure 2e). The final step is to form Ti/Au n-metal pads and also Ti/Au p-metal tracks, each connected with an individual Ni/Au submicron-stripe (Figure 2f). Note that SiO_2 has dual functions. The first function is to confine the emission exactly within the SiO_2 window. Secondly, and more importantly, the SiO_2 layer is an ideal site for p-metal tracks to be directly contacted with the Ni/Au submicron-stripes, eliminating the complex registration steps which would be necessary if the metal track should be contacted with Ni/Au submicron-stripes within the SiO_2 window (The challenge in this particular geometry is the fabrication of top metallic contacts to the submicron-stripes in a way that the contact does not short directly to P-GaN. if the p-metal track is

contacted with Ni/Au submicron-stripes on p-GaN directly, parasitic light will be generated from the p-metal track edge as well. Thus an extra isolation layer is needed prior to the deposition of p-metal tracks. In order to contact with Ni/Au submicron-stripes on p-GaN, the isolation material on top of the Ni/Au submicron-stripes needs to be selectively removed. Due to the submicron feature size however, this would need the use of accurate pattern registration techniques, for instance, electron-beam lithography, which does not lend itself to large-scale fabrication). Thus our strategy here can significantly simplify the submicron-stripe LED fabrication procedure.

Shown in **Figure 3**a is the SEM image of Ni/Au nanostipes formed by LED writing of the resist followed by metal lift off. A portion of the fully processed device is shown in Figure 3b, where the p-metal tracks connected with each submicron-stripe, sitting on the SiO_2 layer, are clearly visible. From the SEM inspection, the minimal width of the Ni/Au submicron-stripe is 900nm, further confirming the sub-micron scale resolution of our LED writing system (see inset in Figure 3b). The actual sizes of the submicron-stripes on the same device range from 900nm to 1.5μm, which are achieved by tuning the moving velocity of the sample stage (**Supporting Information, Figure S3**). The variable velocity of the sample moving stage in turn changes the exposure dose. Thus the feature size can be tuned. Device performances of a serial of LEDs with different sizes are then evaluated by fully gluing the chip onto a ceramic package followed by wire bonding. Shown in Figures 3c-d are optical images of one submicron-stripe LED and two submicron-stripe LEDs switched on at an injection current of 1mA, respectively, clearly revealing the individually addressable capability of each submicron-stripe LED. Under this current injection level, the submicron-stripe LED emission is bright enough to be observed by naked eye. Furthermore, the current spreading is quite uniform along the stripe, even though the contact region is very small.

Shown in **Figure 4**a is representative I-V and optical power plots of a submicron-stripe LED with the narrowest width of 900nm. Clearly the I-V shows very good rectification behavior above turn-on. The turn-on voltage is around 3V, comparable to conventional broad-area LED. Note that the injection current can be up to 3mA, a few orders higher than those previously reported nanoLEDs [3,7,10,16]. Two terminal transport measurements indicate the I-V between 2 adjacent submicron-stripes is linear (after annealed at 400℃) whereas it is non-linear for as-deposit submicron-stripes (i.e., before annealing). Meanwhile the current flowing through the metal submicron-stripe itself (by putting two metal pads at two ends of the metallic submicron-stripe) is much higher than the current between two adjacent submicron-stripes, as shown in figure 4b. These results indicate p-n junction dominates the transport behavior, and that an ohmic contact of the Ni/Au submicron-stripes to p-GaN has formed after annealing. This argument is further strengthened by the TLM results (**Supporting Information, Figure S4**). A specific contact resistance of $1.83\times10^{-4}\,\Omega\cdot cm^2$ is achieved under this annealing condition. Thus, the good electric property of the annealed submicron-stripe device is attributed to the low contact resistance, although the contact area is small. By contrast, the non-annealed submicron-stripe device can emit light as well, but the I-V is really poor, and the emission suffers from serious non-uniformity (**Supporting Information, Figure S5**).

To evaluate the emission brightness, a silicon detector is brought into contact with the top surface of a submicron-stripe device with the narrowest width. The measured optical power for this submicron-stripe LED is up to nearly 28μW, as shown in Figure 4a. The corresponding wall-plug efficiency, which is defined by the ratio between the output power and input power, is 0.1%. This efficiency value is remarkably lower than that of the state-of-the-art commercial LEDs emitting at the same wavelength. Nevertheless,

to the best of our knowledge, this is the first reported optical power for nanoscale emitters. The low wall-plug efficiency is possibly attributed to the lower annealing temperature and the relatively thicker Ni/Au (10nm/20nm) metal layers than commonly used[22], both resulting in a poor transmittance. The wall-plug efficiency can be also underestimated, considering the fact that only the light in the forward direction is collectec by the detector. However, it is essential to deposit a relatively thicker metal layer to warrant good step coverage at the SiO_2 window. In fact, we encountered the problem that the Ni/Au submicron-stripes of the same thickness tends to be broken at the SiO_2 step if they are annealed at a higher temperature of 500℃, possibly due to the different expansion behavior of the metal layer at the SiO_2 sidewall and on p-GaN.

Despite the low absolute wall-plug efficiency, one intriguing observation is that the droop behavior of the normalized external quantum efficiency (EQE) with injection current density is remarkably suppressed for submicron-stripe LEDs, as shown in Figure 4C. In fact, the EQE continuously increases, reaches its peak value at a current density of 100A/cm^2, and then it begins to drop, but obviously slower than the conventional broad-area LED. Even though the current density reaches 1000A/cm^2, the efficiency is only dropped about 40%. By contrast, for the reference broad-area LED, the efficiency reaches its maxima at 2A/cm^2, and then up to 80% droop of the efficiency occurs at 100A/cm^2. The suppressed efficiency droop phenomenon has been observed in GaN nanowire light-emitting diodes[23,24], and it has been explained by a consequence of the suppressed electron overflow, or the low epitaxial defect density. We argue here, however, different mechanisms are responsible for the observed efficiency droop effect in our submicron-stripe LEDs. Both the submicron-stripe LED and the reference broad-area LED are made from the same wafer with the same electron block layer. Thus the suppressed electron overflow is unlikely to be the main mechanism for the efficiency droop, neither is the epitaxial defect density. The planar submicron-stripe LED, however, has minimized plasma-induced damage, compared with the reference LED, given that the emission area defined by the submicron-stripe electrode is not etched, and the etched area n-GaN is far away from the submicron-stripe. This means plasma-damage assisted Auger recombination, if it exists, is suppressed in the submicron-stripe LED. The more uniform current spreading in smaller LED structures is possibly another main mechanism responsible for the suppressed efficiency droop at the high current density [25,26]. Finally, but not the least, the lower junction temperature in the submicron-stripe LED, as determined from the current-dependent EL spectra shown in Fig.5, may be also responsible for the reduced efficiency droop [27].

To examine if the submicron-stripe LED has robust operation, aging tests are conducted for the 900nm stripe device at an injection current of 1mA for 48 hours. As shown in figure 4d, the optical power of the device is only decreased by 2% (from 11.5 μW to 11.2 μW). Considering that the injection current density is very high (1100A/cm^2), the device reliability is thus very good. This again, can be attributed to the low specific contact resistance. Pixel to pixel uniformity in terms of the optical power output is also evaluated, indicating the overall uniformity is good (**Supporting Information, Figure S6**). I-V and power characteristics of the nanoLEDs with different sizes ranging from 0.9μm to 1.5μm are also examined, as shown in Figure 5. It is clearly observable that both the absolute output power and the injection current increase with the LED size (Figure 5a-b). However, the optical power density and current density of the devices with different sizes show no significant difference (Figure 5c-d). This is not surprising, as the device width is still bigger than DeBroglie wavelength. Furthermore, the submicron-stripe LED device is essentially a planar device, and the carriers are not physically confined in a nanoscale p-n junction. Thus, there is no quantum size effect, which

could be observed in much smaller nanostructures such as quantum wires [28] and quantum dots [29].

Shown in **Figure 6**a is the current density dependent EL spectra of the 900nm sized LEDs. The EL peak position shows a very weak blueshift (of ~2nm) upon increasing the injection current density from 0.5A/cm^2 to 330A/cm^2. By contrast, the peak position of a conventional broad-area LED (280μmx320μm) blueshifts in the beginning but then redshifts when the injection current density is above 110A/cm^2, as shown in Figure 6b. It is well known that the blueshift of the emission wavelength is attributed to the so-called band-filling effect or the screening of Quantum Stark Effect [30], whereas the redshift is due to self-heating-induced bandgap shrinkage [31]. Thus, the absence of redshift of the emission for nanoLEDs is due to the lower junction temperature under the same current density, leading to a better spectral stability (with the injection current density). This viewpoint is further validated by the peak wavelength measurement result under pulsed condition, as shown in Figure 6c. For the nanostripe device, the peak-wavelength vs current density plot under DC condition is basically the same as under pulsed condition. However, for the reference broad-area LED, the redshift of the peak wavelength, which is clearly observable under DC operation, doesn't present any more under the pulsed condition. These results unambiguously indicate the self-heating effect or the junction temperature in the nanostripe device is minimized (within this current density range). Shown in Fig.6(d) are the measured junction temperatures of the submicron-stripe LED and conventional broad-area LED, respectively, based on the well-established spectral-shift method [32]. Indeed, the junction temperature rise for the submicron-LED is much slower with increasing the current density, further validating our above auguments. We notice the observed spectral shift trend of nanoLEDs is also similar to those LEDs with sizes falling within the micro-scale region [32,33].

Spatial resolution of the submicron-stripe LED emission is then examined by using a high-resolution CCD camera. Shown in **Figure 7**a, for instance, is a CCD-captured optical image of the 900nm-sized nanoLED operated under an injection current of 0.6mA. The lateral emission width is broadened to 3μm under this condition. The actual emission size is dependent on the current injection level, as shown in Figure 7b. The emission width is increased from 2.5μm to 5μm and then saturated upon increasing the current from 0.1mA to 3mA. The reason for this is that the carrier recombination cannot be physically confined by the region below submicron-stripe metallic contact. Unlike organic semiconductors, the mobility of charge carriers in inorganic semiconductors is high enough to allow lateral diffusion of the carriers through p-GaN. When the injection current level is relatively low, the region defined by the submicron-stripe has a lower resistance and thus the current is mainly vertically injected. However, when the injection current is high, current can spread laterally, resulting in a wider emission. These two scenarios are schematically depicted in Figure 7b.

To further understand the current-dependent emission size, numerical simulation of the current spreading under different current injections is conducted [34]. In the simulation, for electrically neutral p- and n regions, drift is the dominant mechanism of the carrier transport and the electron-hole recombination in this region is neglected. Current spreading in these regions is described by the Ohm law equation.

$$\boldsymbol{j} = (\boldsymbol{\sigma}/q)\nabla F \quad , \quad \boldsymbol{\mu} = \begin{pmatrix} \mu_\perp & 0 & 0 \\ 0 & \mu_\perp & 0 \\ 0 & 0 & \mu_\parallel \end{pmatrix} \qquad (1),$$

where $\boldsymbol{\sigma} = q\boldsymbol{\mu}N_i^{\pm}$ is the conductivity tensor of the epilayer, q is the electron charge, $\boldsymbol{\mu}$ is the mobility tensor accounting for possible difference between the in-plane ($\mu_\perp$) and normal ($\mu_\parallel$) carrier mobilities, $N_i^{\pm}$ ($i = D, A$) is the ionized impurity (donor or acceptor) concentration equal to the carrier (electron or hole)

concentration in the layer due to the electric neutrality, and F is the quasi-Fermi level of the respective carriers. On the other hand, for the p-n junction (active region), the relationship between the current density j and the bias U_b is defined by the expression followed from the Shockley's diode model:

$$U_b = \frac{mkT}{q} ln \frac{j + j_0 exp\left(-E_G/_{kT}\right)}{j_0 exp\left(-E_G/_{kT}\right)} + j\rho_A \quad (2).$$

Here, q is the electron charge, k is the Boltzmann constant, m is non-ideality factor, j_0 is saturation current density, E_G is the bandgap of the InGaN alloy, T is the junction temperature, and ρ is serial resistance of the active region. Thus, current spreading can be solved on a 3D-grid based on the above equations, using advanced numerical algorithms. A more detailed description of the current spreading modelling can be found in the software manual [34]. Figures 7c-d, for instance, show the simulated current spreading of the active region for a 900nm-wide submicron-stripe LED under injection current of 1mA and 3mA, respectively. Consistent with our prediction, it is obvious from the simulation that the current spread laterally at the higher injection current. This means a real planar nano-emitter would require the further reduction of the metallic contact size (to 200nm or less, if we assume the emission is broadened by 5 times), which however, is beyond the capability of our current LED writing system. Alternatively, deactivation of the p-GaN conductivity (to reduce the carrier mobility) would expect to be effective as well for restricting the lateral current spreading for submicron-stripe LEDs. These investigations are undergoing and will be reported elsewhere.

Finally, we'd like to address, while in our LED writing system, a CMOS-driven LED array is used as the writing source, which may lead to higher costs of the system, it is entirely feasible to drive such LED arrays using other simpler driving techniques[35]. CMOS-driving does have some merits though, for instance, it can deliver sub-nanosecond pulses, making pulsed exposure possible. This enables us to more flexibly control the exposure dose, and thus generate more complicated patterns (for instance, a resist line with variable width) using one single exposure.

Conclusions

In summary, we have demonstrated a novel technique to manufacture high-performance submicron-stripe LED arrays based on direct LED writing. The submicron-stripe LEDs have individually addressable capability, precise size and position control, and good electric performances. Although the emission size is broadened because of the lateral carrier diffusion, these submicron-stripe LED arrays can find many applications such as bio-photonics and single molecular excitation, where the robust device operation, individually-addressable capability, and programmable emission pattern of the light source outweigh the emission size. Furthermore, the submicron-stripe device size can be reduced by further improving the writing resolution of the current LED writing system, opening up the good opportunity to manufacture real nano-emitters with nanoscale emission sizes.

Methods

LED wafer structures: the submicron-stripe LED arrays are fabricated from commercially available 460 nm wafers grown on c-plane sapphire substrates. The LED structure consists of 3 μm of undoped GaN, 2.5 μm of Si-doped GaN, and a 150 nm InGaN/GaN multi-quantum well for emission at 460 nm, topped with a 0.15 μm Mg-doped GaN epilayer.

Fabrication of the submicron-stripe LED arrays: The fabrication starts by depositing 300nm SiO_2 onto the LED sample using plasma enhanced chemical vapor

deposition (PECVD; Oxford) at 300℃. a 100μm× 6mm resist window is then formed by spin coating 2 μm -thick S1818 resist at a speed of 4000rpm followed by conventional optical lithography (baking temperature and time: 115℃, and 1min; exposure time: 7.5s; development time: 40s). wet etching of the underneath SiO_2 layer for 1.5min using commercial etchant (BOE 7:1) at room temperature and then remove the resist pattern by acetone, leading to the formation of a SiO_2 window on the LED wafer. Afterward, the sample is coated with a 0.5μm S1805 resist layer at a speed of 4000rpm followed by soft baking at 115℃ for 1min. Subsequently, LED writing is conducted to create 120 resist trenches (pitch: 50 μm) using the smallest pixel (14 μm in diameter) to expose the S1805 resist followed by washing away the exposed resist. By varying the velocity of the sample moving stage, resist trenches with width of 0.9 μm to 1.5 μm can be achieved. The following step is to load the sample into an evaporator (Edward) for 10nm Ni/ 20nm Au deposition, followed by standard metal lift off by using acetone. Drying the sample by put it on a hotplate for 5min. at 115℃, the sample is then loaded into the chamber of a rapid thermal annealing (RTA) system for the formation of p-type ohmic contact (5min. at 400℃; air atmosphere). The next step is to expose the n-GaN layer by ICP (STS) etching for 70s using a 2-μm S1818 resist pattern defined by optical lithography. Followed by S1818 resist removal using acetone, another 4.5 μm thick SPR220 resist layer is coated and patterned by optical lithography. Finally, the sample is loaded into a sputter for 50nm Ti/ 200nm Au deposition followed by metal lift off, to form n-contact pads, and also the p-metal tracks connected with each submicron-stripe.

Measurement of specific contact resistance (see also Figure S4 in supporting information): standard circular transmission line patterns with different spacing ranging from 10μm, 15μm, 20μm, 25μm, 30μm, 35μm, and 40μm to 45 μm are formed on a GaN LED reference sample by optical lithography and metal lift off (Ni 10nm/Au 20nm). The reference sample is then loaded into RTA, together with the submicron-stripe LED sample, for annealing to form ohmic contacts. The annealing condition is 400℃ for 5 minutes under air. Specific contact resistance is then extracted by using the following equations:

$$R = \frac{R_S}{2\pi}\left[\ln\left(\frac{r_1}{r_0}\right) + L_T\left(\frac{1}{r_1} + \frac{1}{r_0}\right)\right] \quad (3).$$

SEM and AFM measurements: an AFM(Accurion XE-100) and a SEM (Hitatchi S4700) are used to characterize the feature size of the LED-written resist patterns, as well as the fabricated submicron-stripe device.

Characterization of electric, optical, and spectral properties: devices were wired bonded onto a ceramic package. A semiconductor parameter analyzer (HP 4155C, Agilent) was used to measure the electrical properties. Electroluminescence measurements of the emission spectra were performed with a spectrometer (Ocean Optics). Optical power measurement was conducted by putting a silicon detector on top of the device. Spatial resolution of the submicron-stripe device emission was analyzed by using a high resolution CCD camera (NA: 0.9)

Acknowledgements

This work was supported in part by the Engineering and Physical Sciences Research Council under Grant EP/D078555/1 and Grant EP/F05999X/1, and by the Special Funds for Innovative Research Team in Guangdong Province, China. We would like to thank Jim Small for his assistance in the SEM measurements. Authors declare no competing financial interest.

Electronic Supplementary Material: Supplementary material (please give brief details, e.g., further details of the annealing and oxidation procedures, STM measurements, AFM imaging and Raman spectroscopy measurements) is available in the online version of this article at http://dx.doi.org/10.1007/s12274-***-****-* (automatically inserted by the publisher).

References

[1] Nakamura, S.; Senoh, M.; Mukai, T. P-GaN/N-InGaN/N-GaN Double-Heterostructure Blue-Light-Emitting Diodes. *Japanese Journal of Applied Physics* **1993**, *32*, L8–L11.

[2] Michaelis, J.; Hettich, C.; Mlynek, J.; Sandoghdar, V. Optical Microscopy Using a Single-molecule Light Source. *Nature* **2000**, *405*, 325–328.

[3] Lu, Y.-J.; Lin, H.-W.; Chen, H.-Y.; Yang, Y.-C.; Gwo, S. Single InGaN Nanodisk Light Emitting Diodes as Full-color Subwavelength Light Sources. *Applied Physics Letters* **2011**, *98*, 233101.

[4] Hayden, O.; Payne, C. K. Nanophotonic Light Sources for Fluorescence Spectroscopy and Cellular Imaging. *Angewandte Chemie* **2005**, *117*, 1419–1422.

[5] Price, S. P.; Henzie, J.; Odom, T. W. Addressable, Large-Area Nanoscale Organic Light-Emitting Diodes. *Small* **2007**, *3*, 372–374.

[6] Veinot, J. G. C.; Yan, H.; Smith, S. M.; Cui, J.; Huang, Q.; Marks, T. J. Fabrication and Properties of Organic Light-Emitting "Nanodiode" Arrays. *Nano Letters* **2002**, *2*, 333–335.

[7] Boroumand, F. A.; Fry, P. W.; Lidzey, D. G. Nanoscale Conjugated-Polymer Light-Emitting Diodes. *Nano Letters* **2005**, *5*, 67–71.

[8] Yamamoto, H.; Wilkinson, J.; Long, J. P.; Bussman, K.; Christodoulides, J. A.; Kafafi, Z. H. Nanoscale Organic Light-Emitting Diodes. *Nano Letters* **2005**, *5*, 2485–2488.

[9] Hayden, O.; Greytak, A. B.; Bell, D. C. Core–Shell Nanowire Light-Emitting Diodes. *Advanced Materials* **2005**, *17*, 701–704.

[10] Liu, C.-Y.; Bard, A. J. Individually Addressable Submicron Scale Light-Emitting Devices Based on Electroluminescence of Solid Ru(bpy)3(ClO4)2 Films. *J. Am. Chem. Soc.* **2002**, *124*, 4190–4191.

[11] Bao, J.; Zimmler, M. A.; Capasso, F.; Wang, X.; Ren, Z. F. Broadband ZnO Single-Nanowire Light-Emitting Diode. *Nano Lett.* **2006**, *6*, 1719–1722.

[12] Zimmler, M. A.; Voss, T.; Ronning, C.; Capasso, F. Exciton-related Electroluminescence from ZnO Nanowire Light-emitting Diodes. *Applied Physics Letters* **2009**, *94*, 241120.

[13] Könenkamp, R.; Word, R. C.; Schlegel, C. Vertical Nanowire Light-emitting Diode. *Applied Physics Letters* **2004**, *85*, 6004–6006.

[14] Motayed, A.; Davydov, A. V.; He, M.; Mohammad, S. N.; Melngailis, J. 365 nm Operation of n-nanowire/p-gallium Nitride Homojunction Light Emitting Diodes. *Applied Physics Letters* **2007**, *90*, 183120.

[15] Duan, X.; Huang, Y.; Cui, Y.; Wang, J.; Lieber, C. M. Indium Phosphide Nanowires as Building Blocks for Nanoscale Electronic and Optoelectronic Devices. *Nature* **2001**, *409*, 66–69.

[16] Makarovsky, O.; Kumar, S.; Rastelli, A.; Patanè, A.; Eaves, L.; Balanov, A. G.; Schmidt, O. G.; Campion, R.; Foxon, C. T. Direct Laser Writing of Nanoscale Light-Emitting Diodes. *Advanced Materials* **2010**, *22*, 3176–3180.

[17]. Kuo, M.-L.; Kim, Y.-S.; Hsieh, M.-L.; Lin, S.-Y. Efficient and Directed Nano-LED Emission by a Complete Elimination of Transverse-Electric Guided Modes. *Nano Lett.* **2011**, *11*, 476–481.

[18] Qian, F.; Gradec□ak, S.; Li, Y.; Wen, C.-Y.; Lieber, C. M. Core/Multishell Nanowire Heterostructures as Multicolor, High-Efficiency Light-Emitting Diodes. *Nano Letters* **2005**, *5*, 2287–2291.

[19] Jeon, C. W.; Gu, E.; Dawson, M. D. Mask-free Photolithographic Exposure Using a Matrix-addressable Micropixellated AlInGaN Ultraviolet Light-emitting Diode. *Applied Physics Letters* **2005**, *86*, 221105.

[20] Guijt, R. M.; Breadmore, M. C. Maskless Photolithography Using UV LEDs. *Lab on a Chip* **2008**, *8*, 1402.

[21] Elfström, D.; Guilhabert, B.; McKendry, J.; Poland, S.; Gong, Z.; Massoubre, D.; Richardson, E.; Rae, B. R.; Valentine, G.; Blanco-Gomez, G. *et al.* Mask-less Ultraviolet Photolithography Based on CMOS-driven Micro-pixel Light Emitting Diodes. *Opt. Express* **2009**, *17*, 23522–23529.

[22]. Cao, X. .; Stokes, E. .; Sandvik, P.; Taskar, N.; Kretchmer, J.; Walker, D. Optimization of Current Spreading Metal Layer for GaN/InGaN-based Light Emitting Diodes. *Solid-State Electronics* **2002**, *46*, 1235–1239.

[23] Guo, W.; Zhang, M.; Bhattacharya, P.; Heo, J. Auger Recombination in III-Nitride Nanowires and Its Effect on

Nanowire Light-Emitting Diode Characteristics. *Nano Letters* **2011**, *11*, 1434–1438.

[24] Nguyen, H. P. T.; Cui, K.; Zhang, S.; Djavid, M.; Korinek, A.; Botton, G. A.; Mi, Z. Controlling Electron Overflow in Phosphor-Free InGaN/GaN Nanowire White Light-Emitting Diodes. *Nano Lett.* **2012**, *12*, 1317–1323.

[25] Ryu, H.-Y.; Shim, J.-I. Effect of Current Spreading on the Efficiency Droop of InGaN Light-emitting Diodes. *Opt Express* **2011**, *19*, 2886–2894.

[26] Tian, P.; McKendry, J. J. D.; Gong, Z.; Guilhabert, B.; Watson, I. M.; Gu, E.; Chen, Z.; Zhang, G.; Dawson, M. D. Size-dependent Efficiency and Efficiency Droop of Blue InGaN Micro-light Emitting Diodes. *Applied Physics Letters* **2012**, *101*, 231110.

[27] Meyaard, D. S.; Shan, Q.; Cho, J.; Fred Schubert, E.; Han, S.-H.; Kim, M.-H.; Sone, C.; Jae Oh, S.; Kyu Kim, J. Temperature Dependent Efficiency Droop in GaInN Light-emitting Diodes with Different Current Densities. *Applied Physics Letters* **2012**, *100*, 081106.

[28] Musin, R. N.; Wang, X.-Q. Quantum Size Effect in Core-shell Structured Silicon-germanium Nanowires. *Phys. Rev. B* **2006**, *74*, 165308.

[29] Padilha, L. A.; Nootz, G.; Olszak, P. D.; Webster, S.; Hagan, D. J.; Stryland, E. W. Van; Levina, L.; Sukhovatkin, V.; Brzozowski, L.; Sargent, E. H. Optimization of Band Structure and Quantum-size-effect Tuning for Two-photon Absorption Enhancement in Quantum Dots. *Nano Lett.* **2011**, *11*, 1227–1231.

[30] Chichibu, S.; Azuhata, T.; Sota, T.; Nakamura, S. Spontaneous Emission of Localized Excitons in InGaN Single and Multiquantum Well Structures. *Applied Physics Letters* **1996**, *69*, 4188–4190.

[31] Cho, J.; Sone, C.; Park, Y.; Yoon, E. Measuring the Junction Temperature of III-nitride Light Emitting Diodes Using Electro-luminescence Shift. *physica status solidi (a)* **2005**, *202*, 1869–1873.

[32] Gong, Z.; Jin, S.; Chen, Y.; McKendry, J.; Massoubre, D.; Watson, I. M.; Gu, E.; Dawson, M. D. Size-dependent Light Output, Spectral Shift, and Self-heating of 400 nm InGaN Light-emitting Diodes. *Journal of Applied Physics* **2010**, *107*, 013103.

[33] Kim, T.; Jung, Y. H.; Song, J.; Kim, D.; Li, Y.; Kim, H.; Song, I.-S.; Wierer, J. J.; Pao, H. A.; Huang, Y. *et al.* High-Efficiency, Microscale GaN Light-Emitting Diodes and Their Thermal Properties on Unusual Substrates. *Small* **2012**, *8*, 1643–1649.

[34] http://www.semitech.us/products/SpeCLED/

[35] Gong, Z.; Zhang, H.X. ; Gu, E. ; Griffin, C. ; Dawson, M.D. ; Poher, V. ; Kennedy, G. ; French, P.M.W. ; Neil, M.A.A.; Matrix-Addressable Micropixellated InGaN Light-Emitting Diodes With Uniform Emission and Increased Light Output. *IEEE Trans. Electron. Dev.* 2007,54, 10, 2650-2658

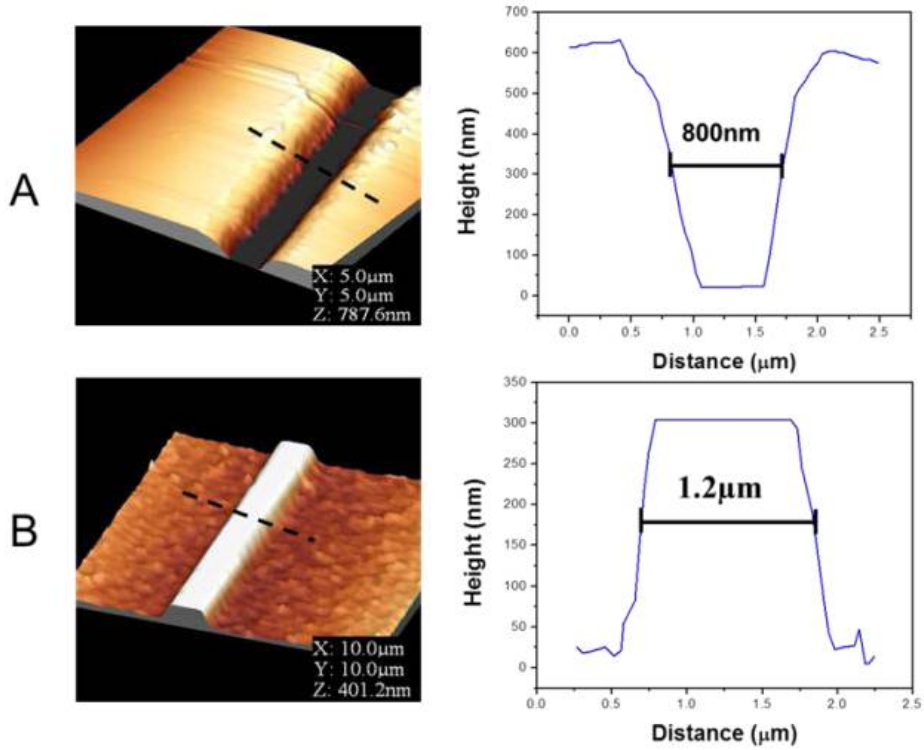

Figure 1. (a) AFM image of a trench written into the positive S1805 resist layer at a velocity of 115μm/s, (b) AFM image of a LED-written stripe formed by negative ma-N405 resist at a velocity of 3μm/s. Cross-sectional profiles along the dash line in (a), and (b) are shown at the right hand side, respectively.

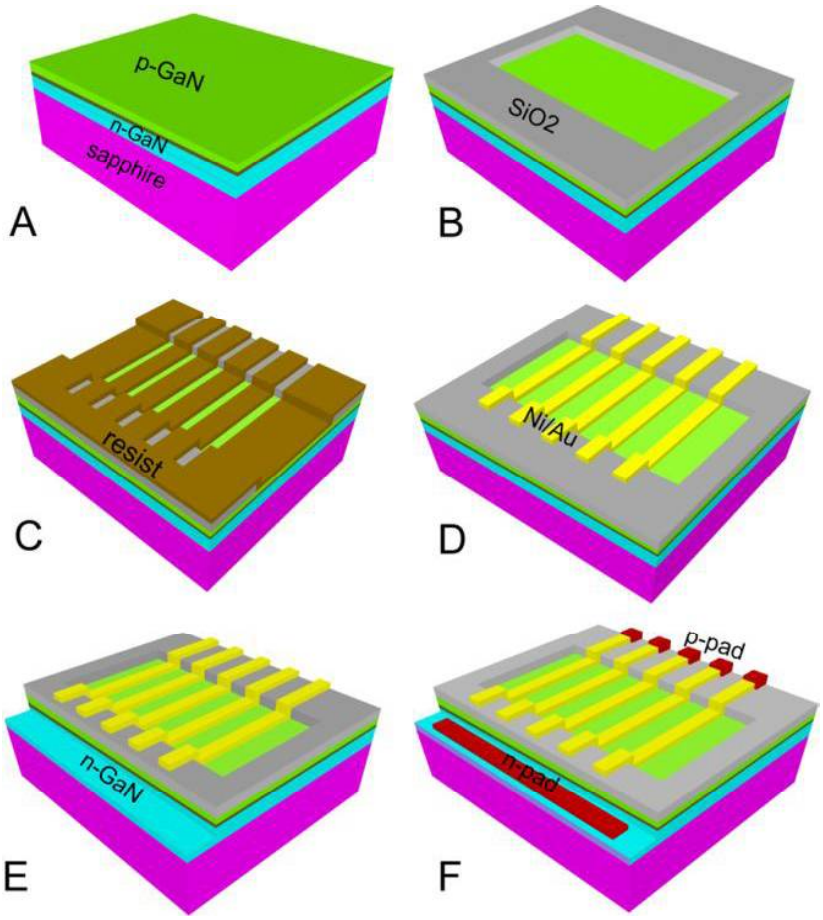

Figure 2. Processing flow for the individually addressable submicron-stripe LEDs based on the LED writing: (a) bare InGaN/GaN wafer, (b) SiO2 window on top of the LED wafer, (c) resist pattern generated by the LED writing system, (d) Ni/Au submicron-stripe formed by evaporating Ni/Au metals onto the resist pattern, (e) exposed n-GaN by ICP etching, and (f) p-metal tracks and n-contact pads formed by sputtering.

.

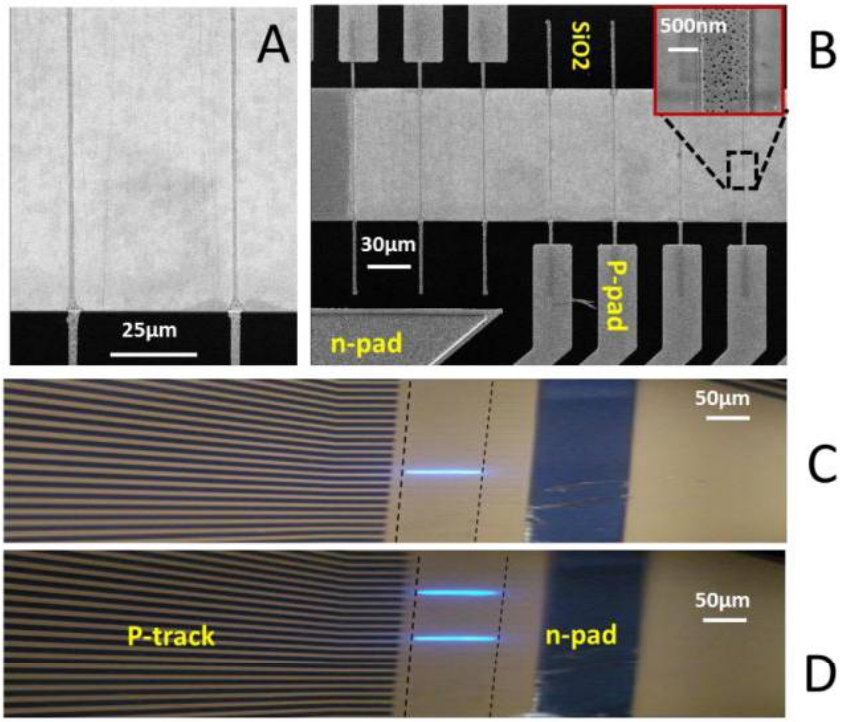

Figure 3. (a) SEM image of the Ni/Au submicron-stripes formed by metal evaporation followed by lift off, (b) SEM image of a fully processed device with integrated p-pads and n-pads, (c) optical image of one submicron-stripe LED switched on, and (d) optical image of two submicron-stripe LEDs switched on. Dash lines in (c) and (d) outline the edge of the SiO2 window. The injection current for devices in (c) and (d) is 1.0mA.

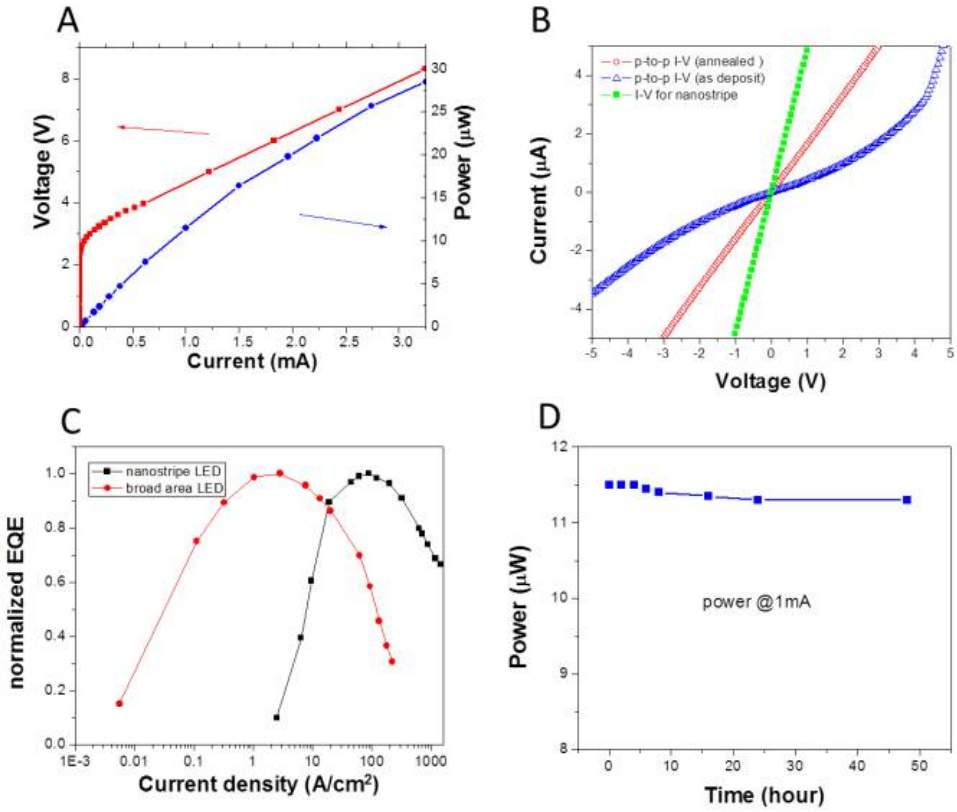

Figure 4. (a) I-V and optical power characteristics of a 900nm-sized submicron-stripe LED, (b) I-V between two adjacent metal submicron-stripes before annealing (blue triangle line), and after annealing (red circle line). The green square line represent the I-V plots through the metallic submicron-stripe itself by putting two metal pads at two ends of the submicron-stripe. (c) Normalized EQE of the 900nm submicron-stripe LED as a function of the current density. For comparison, the corresponding EQE of a conventional broad-area LED as a function of the current density is also included. The pulse width is 0.5ms, and duty cycle is 1%. (d) Optical power of the submicron-stripe LED as a function of the aging time. The injection current for the submicron-stripe LED is 1mA.

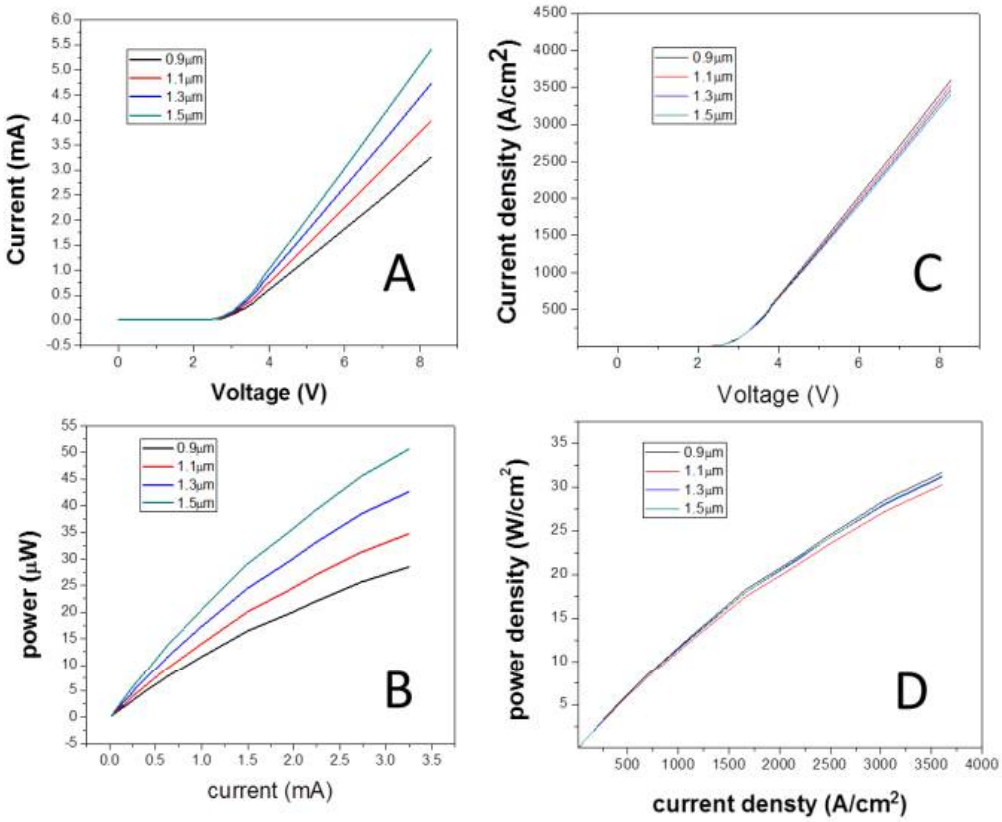

Figure 5. (a) I-V plots for different submicron-stripe device width; (b) power vs current plots for different submicron-stripe width; (c) current density vs forward bias plot for different submicron-stripe width; (d) power density as a function of the current density for different submicron-stripe width.

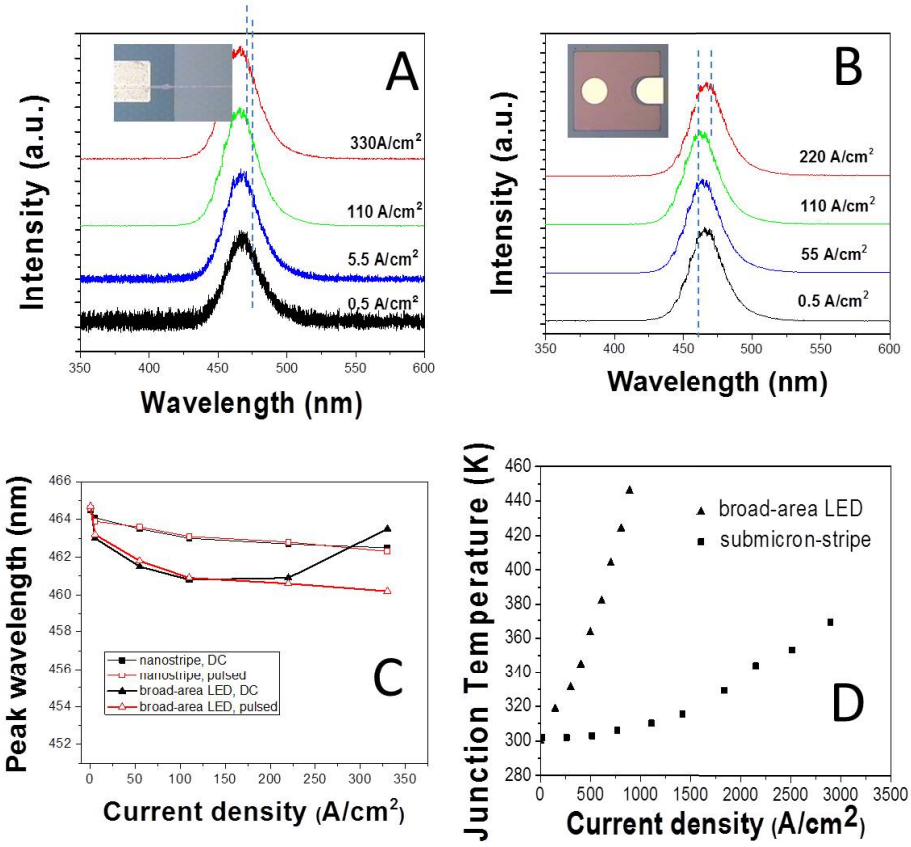

Figure 6. Current-density-dependent EL spectra for (a) the 900nm-sized submicron-stripe LED, and (b) a conventional broad-area LED (280μmx320μm). (c) The peak wavelength position as a function of the current density for the submicron-stripe LED and the reference broad-area LED under DC and pulse operation, respectively. The pulse width is 0.5ms and the duty cycle is 1%. **(d) Measured junction temperature as a function of the current density.**

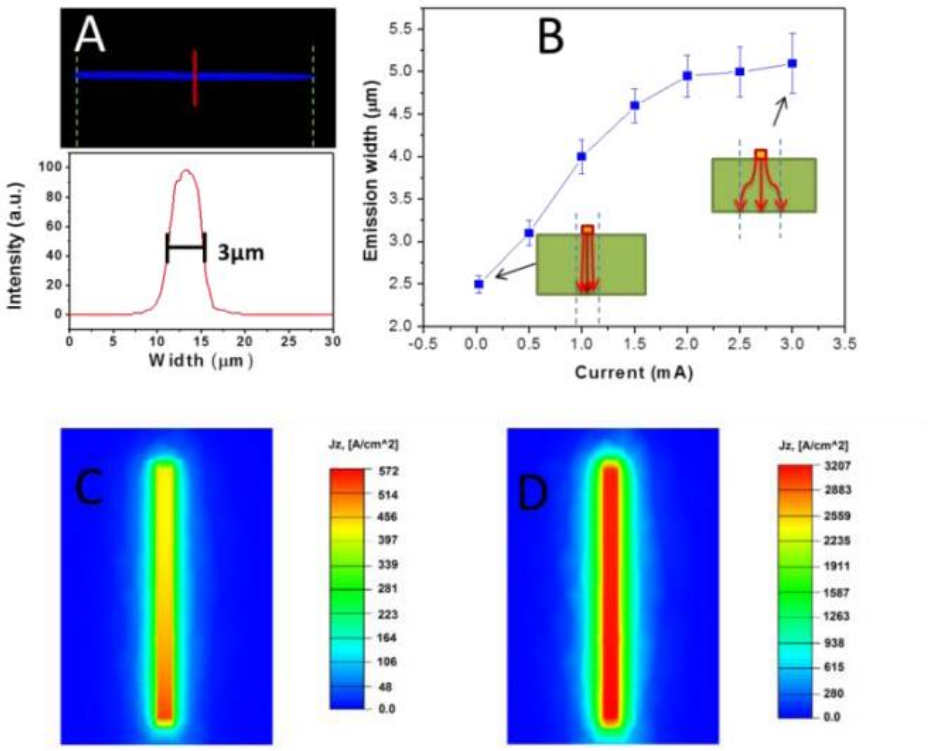

Figure7. (a) CCD-captured image of the 900nm-sized submicron-stripe LED under operation at an injection current of 0.6mA. Dash lines in (a) corresponding to the edge of the SiO2 window. Below the image shows the spatial profile of the emission intensity of the nanooLED along the red line in the image, (b) lateral emission width as a function of the injection current. Two schematics are also included in (b) for illustrating the current spreading issues under low current injection and high injection, respectively. Simulated in-plane current distribution for the 900nm submicron-stripe device under different current injections: (c) 0.6mA, and (d) 3.0mA. The simulation results clearly reveal the wider current spreading under higher injection current.

Nano Res.

Electronic Supplementary Material

Direct LED writing of submicron resist patterns: towards the fabrication of individually-addressable InGaN submicron-stripe LED arrays

Z. Gong[a,b,c](✉), B. Guilhabert[a], Z.T. Chen[b] , and M.D. Dawson[a]

[a] *Institute of Photonics, University of Strathclyde, Wolfson Centre,106 Rottenrow, Glasgow G4 0NW, UK.*

[b] *Guangdong General Research Institute for Industrial Technology, No.363,Changxin Road, Tianhe District, Guangzhou 510650, China*

[c] *Current address: mLED Ltd., 50 Richmond Street,Glasgow G1 1XP, UK. Email: Zheng.gong@mled-ltd.com*

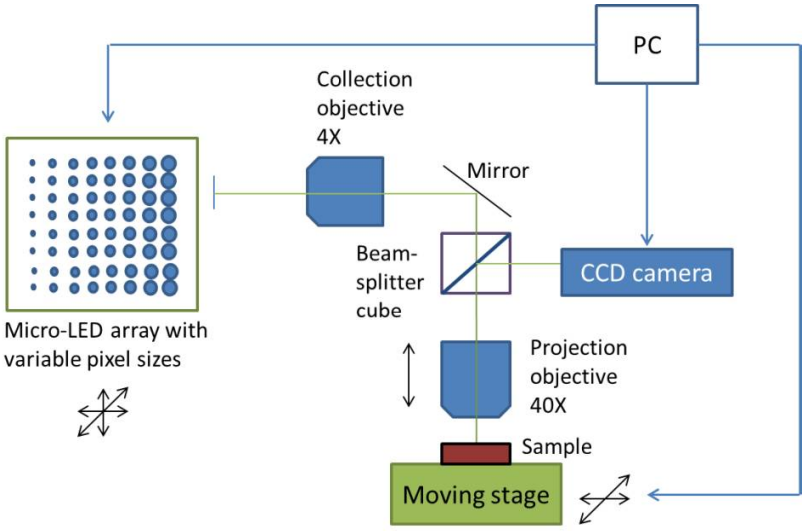

FS1. Schematic setup of the LED array writing system

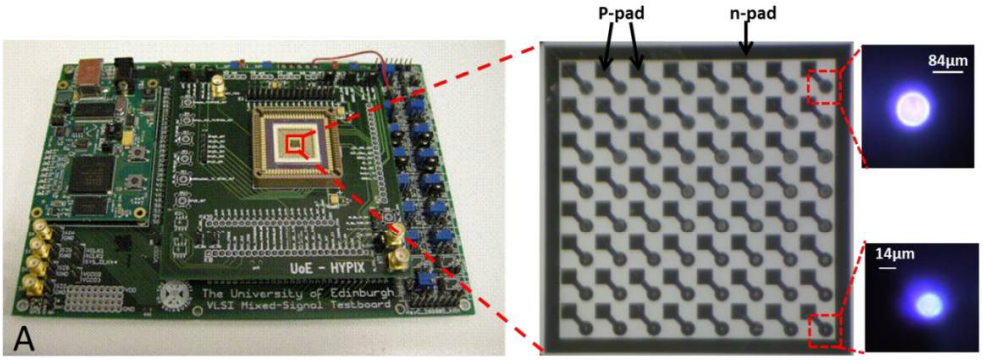

FS2. (a) Optical image of a 8x8 CMOS-driven LED array used in the LED writing system. The diameter of the LED pixels in each column varies from 14μm to 84μm.

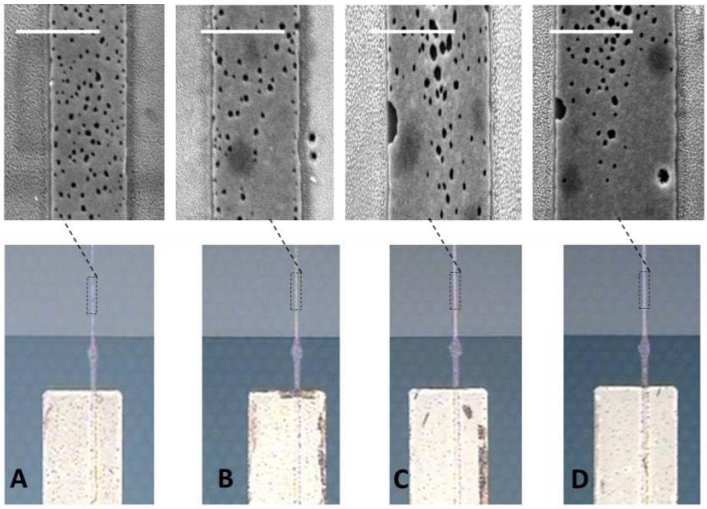

FS3. Ni/Au Submicron-stripe with different widths achieved by the LED writing system by varying the velocity of the sample moving stage: (a) 0.9μm, (b)1.1μm, (c) 1.3μm, and (d) 1.5μm. Scale bar is 1μm.

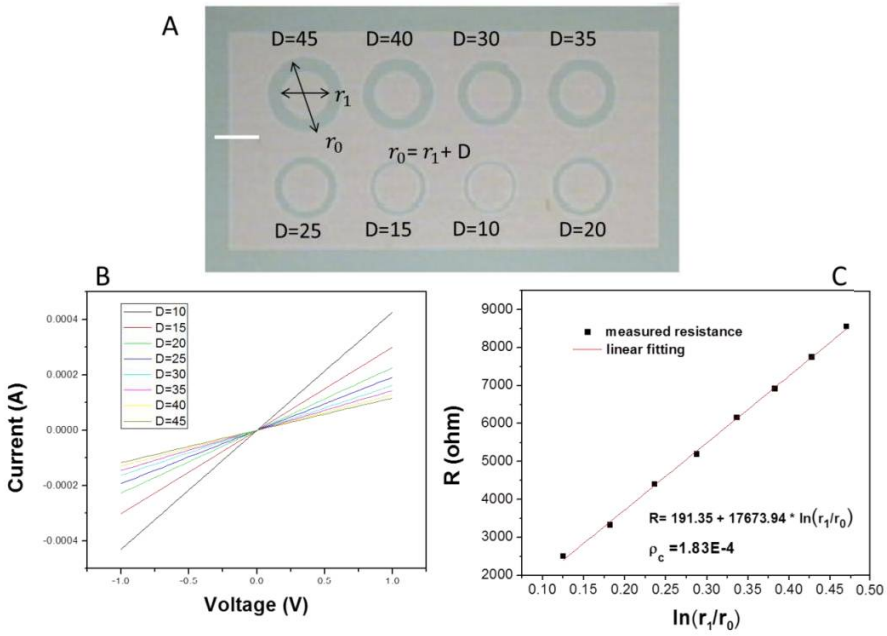

FS4. Contact resistance characterization base on the standard transmission line method: (a) optical image of the circular transmission line patterns with different spacing ranging from 10μm to 45μm, (b) I-V plots for different spacing, and (c) Resistance (R) as a function of ln(r1/r0) . the extracted specific contact resistance from (c) is 1.83E-4 Ωcm^2 .

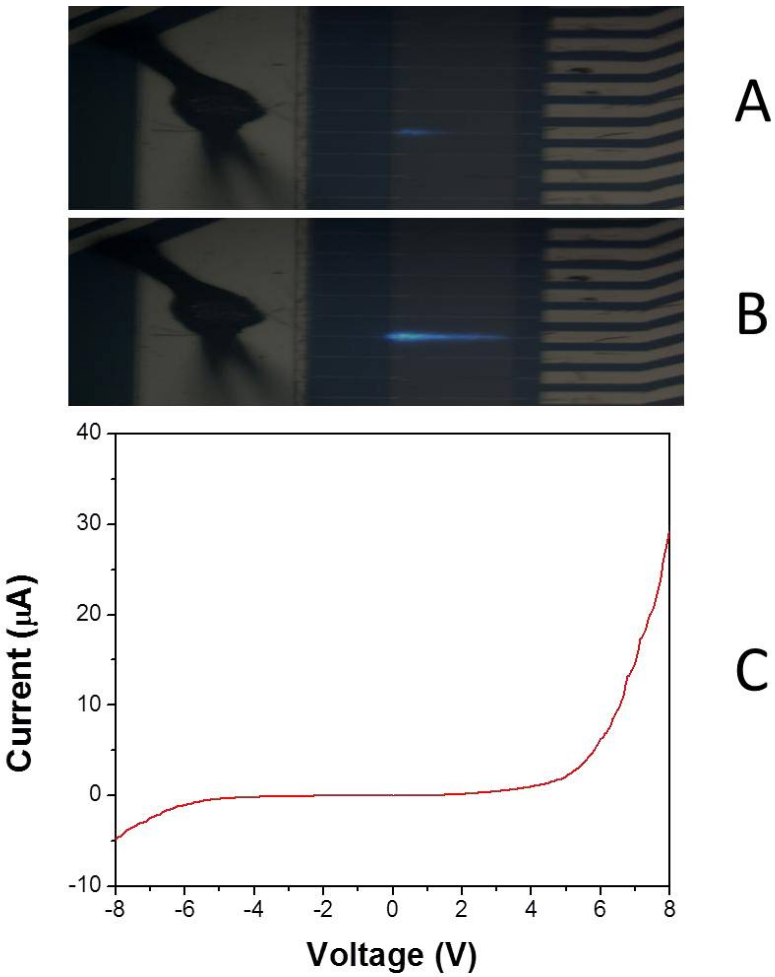

FS5. Emission and I-V characteristics of a LED with as-deposited Ni/Au submicron-stripes without annealing. (a) Emission image of a submicron-stripe device at 20μA, (b) emission image of the same device at 40μA, and (c) corresponding I-V plot of the same device. The emission shows obvious non-uniformity, and the current is crowded to the n-pad. The I-V shows rectification behavior, but the submicron-stripe contact is not ohmic based on the I-V. Note that the current level is at least one order lower than the annealed device.

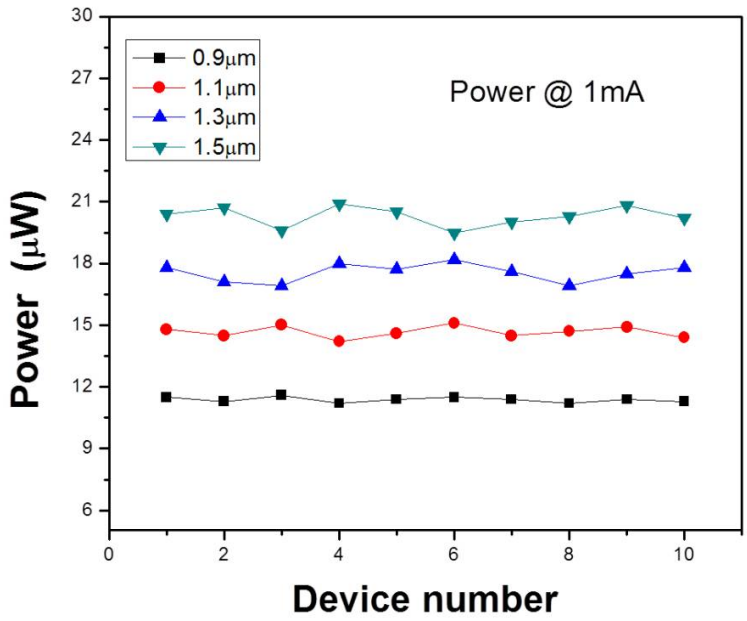

FS6: Optical power as a function of the device number for different submicron-stripe device widths. Optical power of 10 devices are measured for each different device width.

Address correspondence to Zheng Gong, email: zheng.gong@mled-ltd.com